

Role of SSW on thermal-gradient induced domain-wall dynamics

M A S Akanda¹ , M T Islam^{1,2,*}  and X R Wang^{3,4,*}

¹ Physics Discipline, Khulna University, Khulna 9208, Bangladesh

² Center for Spintronics and Quantum Systems, State Key Laboratory for Mechanical Behavior of Materials, Xi'an Jiaotong University, No. 28 Xianning West Road Xi'an, Shaanxi 710049, People's Republic of China

³ Physics Department, The Hong Kong University of Science and Technology, Clear Water Bay, Kowloon, Hong Kong, People's Republic of China

⁴ HKUST Shenzhen Research Institute, Shenzhen 518057, People's Republic of China

E-mail: torikul@phy.ku.ac.bd and phxwan@ust.hk

Received 26 December 2022, revised 15 April 2023

Accepted for publication 24 April 2023

Published 9 May 2023



Abstract

We study the thermal gradient (TG) induced domain wall (DW) dynamics in a uniaxial nanowire in the framework of the Stochastic-Landau-Lifshitz-Gilbert equation. TG drives the DW in a certain direction, and DW (linear and rotational) velocities increase with TG linearly, which can be explained by the magnonic angular momentum transfer to the DW. Interestingly, from Gilbert damping dependence of DW dynamics for fixed TG, we find that the DW velocity is significantly smaller even for lower damping, and DW velocity increases with damping (for a certain range of damping) and reaches a maximal value for critical damping which is contrary to our usual desire. This can be attributed to the formation of standing spin wave (SSW) modes (from the superposition of the spin waves and their reflection) together with travelling spin wave (TSW) modes. SSW does not carry any net energy/momentum to the DW, while TSW does. Damping α compels the spin current polarization to align with the local spin, which reduces the magnon propagation length and thus α hinders to generate SSWs, and contrarily the number of TSWs increases, which leads to the increment of DW speed with damping. For a similar reason, we observe that DW velocity increases with nanowire length and becomes saturated to maximal value for a certain length. Therefore, these findings may enhance the fundamental understanding as well as provide a way of utilizing the Joule heat in the spintronics (e.g. racetrack memory) devices.

Keywords: magnetic domain wall dynamics, Gilbert damping, standing spin waves, magnonic spin transfer torque

(Some figures may appear in colour only in the online journal)

1. Introduction

Achieving fast and energy-efficient controlling of domain wall (DW) in magnetic nanostructure has drawn much attention because of its potential applications in spintronics devices

such as in data storage devices [1–3] and logic operations [4, 5]. Conventionally, there are several steering knobs, namely, magnetic fields [6–11], microwaves [12–15], and spin-polarized currents [16–19], to steer DW in magnetic nanostructures. But these steering knobs are suffering from certain limitations in device applications. Particularly, under an external magnetic field, DW propagation is achieved due to energy dissipation for Gilbert damping. The DW velocity is

* Authors to whom any correspondence should be addressed.

proportional to the rate of energy dissipation, which is estimated by the DW structure [7, 8]. However, the magnetic field is not able to drive DWs synchronously [9, 10, 20]. Whereas a spin-polarized current is able to drive a DW, or a series of DWs in a certain direction with the mechanism of spin-transfer torque (STT) [21–24]. But, the requirement of high current density is a bottleneck as it, due to Joule-heating, leads to the rising of temperature of the device significantly [16, 17, 20]. Consequently, the devices are suffering from stability, error rate and lifetime issues [25]. To overcome these challenges, spin-wave spin current or magnons generated by the thermal gradient (TG) emerges as a potential way of inducing DW motion [26, 27]. The recent studies [28, 29] reported that TG can generate a spin-voltage or the spin-wave spin current in a ferromagnetic nanowire which shows the possibility to lengthen the lifetime, reduce the error rate and improve the stability of the memory device by harvesting the Joule heat. Purposely, considering the thermal effects as a driving force, it is necessary to improve the transport theories based on the interplay among charge, spin and heat current [26]. Therefore, the study of TG-driven DW dynamics is significant not only for spintronics device applications but also for intuitive physics comprehension of how the spin-wave spin current interacts with magnetic DW [30, 31]. Presently, in order to attribute the physical mechanism of the TG-driven DW dynamics, two theories of different origins are prevailing, namely, microscopic (magnonic theory) theory [32–36] and macroscopic (thermodynamic theory) theory [37–40]. According to the microscopic theory, under TG, the magnons are generated in the region of higher temperature and propagate to the lower temperature region, and thus a magnonic spin current is induced. During the passing of magnons through the DW, magnons give a magnonic STT on the DW. Thus, TG drives the DW toward the hotter region (opposite to the direction of magnonic spin current) of the nanowire [30, 34, 41]. On the other hand, the thermodynamic theory says that, in order to get the system with minimal free energy, TG generates an entropic force which leads the DW to the hotter end [37, 38].

However, recent studies demonstrated that the TG-induced magnons could drive the DW either towards the hotter region if the magnons are transmitted [33, 35, 41, 42] or towards colder region if the magnons are reflected [36, 43, 44] from the DW. Magnon reflection or transmission relies on magnon frequency [32], the system under investigation [42] and Dzyaloshinskii–Moriya interaction [44]. In the case of the DW propagation toward the hotter region, TG (which generates spin-wave spin current) induces DW propagation due to magnonic STT rather than the energy dissipation [42]. So, the physical reason for the DW motion is the magnonic STT (carried by spin-wave spin current) to the DW. Under this physical mechanism, i.e. TG, the fast and energy-efficient DW speed significantly relies on the damping coefficient since it is related to the propagation length of spin waves. For the lower damping, the propagation length is larger. Hence the DW speed is larger which is desired for device applications. However, for lower damping, there is a probability of exciting the standing spin waves (SSWs),

which do not carry net energy/momentum, together with the travelling spin waves (TSWs) in the nanowire of finite length. Therefore, it is meaningful to understand how the excited spin wave modes for different α and nanowire length can affect the DW dynamics along a nanowire under TG. We found that the DW propagates toward the hotter region of the nanowire with accompanying DW-plane rotation around the easy x -axis. The DW (linear and rotational) speeds increase with TG linearly. These observations can be attributed to the mechanism of the magnonic STT to the DW [32, 33, 42]. Interestingly, we observed that the DW speed increases with α (for the range of $\alpha \sim 0.0005$ to 0.001), and it reaches a maximal value for certain damping, referred to as critical damping (α_c). With a further increment of α , DW speed decreases monotonically. Usually, the DW speed should decrease with α , since the spin-wave/magnon propagation length is inversely proportional to α . However, for a lower α , DW speed is smaller. This is because, with lower α , the formation of more SSWs (from the superposition of spin waves and their reflection at the boundary) rather than the TSWs. The SSW does not carry any spin angular momentum/magnonic STT to the DW, while the TSW does. With the increment of α (from 0.0005 to 0.001), DW speed shows an increasing trend. This is because the magnon propagation length decreases with α , and thus α hinders to generate the SSWs, and contrarily the TSWs increase, which leads the increment of DW speed. We also observed that DW speed v_{simu} increases with nanowire length (L_x) and becomes saturated to maximal (indicated by horizontal dotted lines) for a certain L_x . The reason is that the distance between two ends increases with L_x so that the spin waves are abated before reflection, i.e. the number of SSWs reduces; contrarily, the number of TSWs increases, and thus DW speed increases. Therefore, the above obtained DW dynamics in nanowires under TG might be useful for the fundamental understanding and to optimize the damping coefficient and nanowire length for applications in spintronics devices.

2. Analytical model and method

We consider a magnetic nanowire (square cross-section) in which, initially, a DW is placed at the center to avoid the boundary effect of the nanowire as shown in figure 1. L_x and $L_y \times L_z$ are length and cross-sectional area of the nanowire, respectively. The DW width Δ is larger than the dimension of L_y and L_z , but much smaller than L_x . The nanowire with square cross-section geometry is referred to as the uniaxial nanowire, which we have studied here. Before applying the TG, we relax the system to a minimal energy state and remove surface charges from the left and right sides of the nanowire. We keep the spin of the left and right edges rigid to obtain a fixed boundary condition. Here, we employ constant TG, rather than localized Gaussian temperature, to obtain steady-state DW dynamics [42]. So, a constant TG, which can be generated by a Peltier Cooler, in reality, [27], is applied along the nanowire. Here, the applied temperature (0 K–716 K (max)) is below

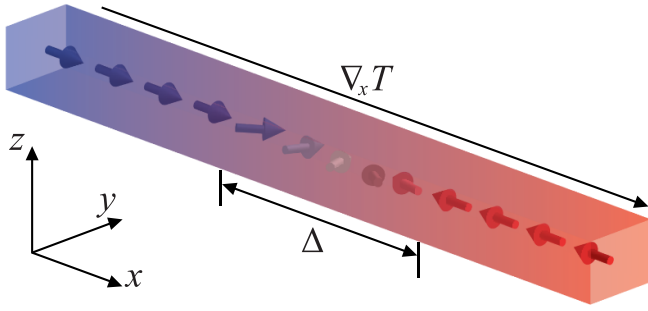


Figure 1. Schematic figure of a magnetic nanowire containing a head-to-head DW at the center of the nanowires under a temperature gradient, $\nabla_x T$. The region of the sample that is colder (hotter) is represented by the blue (red) color.

the Curie temperature T_c . Since the main focus of this study is to investigate the magnonic effects on DW dynamics under TG, we consider the spin waves explicitly. The material parameters, namely, exchange constant, crystalline anisotropy, saturation magnetization, and Gilbert damping are assumed to be constant. Indeed, the atomistic magnetic moments do not change much with temperature. At the atomistic level, the exchange constant (which comes from the Pauli-exclusion-principle) and the crystalline anisotropy (which comes from the spin-orbit-coupling) weakly rely on the temperature due to the vibration of atoms [42, 45].

The magnetization dynamics is governed by the stochastic Landau–Lifshitz–Gilbert (LLG) equation [46–48],

$$\frac{d\mathbf{m}}{dt} = -\gamma \mathbf{m} \times (\mathbf{h}_{\text{eff}} + \mathbf{h}_{\text{th}}) + \alpha \mathbf{m} \times \frac{\partial \mathbf{m}}{\partial t}, \quad (1)$$

where $\mathbf{m} = \mathbf{M}/M_s$ is the magnetization direction, M_s is the saturation magnetization, α is the Gilbert damping coefficient, and γ is the gyromagnetic ratio. $\mathbf{h}_{\text{eff}} = \frac{2A}{\mu_0 M_s} \sum_{\sigma} \frac{\partial^2 \mathbf{m}}{\partial x_{\sigma}^2} + \frac{2K_x}{\mu_0 M_s} m_x \hat{\mathbf{x}} + \mathbf{h}_{\text{dipole}}$ is the effective field, where A is the exchange stiffness constant, x_{σ} ($\sigma = 1, 2, 3$) denote Cartesian coordinates x, y, z , K_x is the easy-axis anisotropy, $\mathbf{h}_{\text{dipole}}$ is the dipolar field, and \mathbf{h}_{th} is the thermal stochastic field.

MUMAX3 (micromagnetic simulation package) [48] has been used to solve the stochastic LLG equation in which we use the adaptive Heun solver. To obtain stability and efficient calculation [42], the time step is chosen 10^{-14} s for the unit cell size $(2 \times 2 \times 2) \text{ nm}^3$. The time step 10^{-15} s is required to choose for unit cell smaller than $(2 \times 2 \times 2) \text{ nm}^3$. The saturation-magnetization $M_s = 8 \times 10^5 \text{ A m}^{-1}$ and exchange-stiffness-constant $A = 13 \times 10^{-12} \text{ J m}^{-1}$ are considered to mimic permalloy in this study. The thermal field follows the Gaussian process characterized by the following statistics [42, 49, 50]

$$\begin{aligned} \langle h_{\text{th},ip}(t) \rangle &= 0, \\ \langle h_{\text{th},ip}(t) h_{\text{th},jq}(t + \Delta t) \rangle &= \frac{2k_B T_i \alpha_i}{\gamma \mu_0 M_s a^3} \delta_{ij} \delta_{pq} \delta(\Delta t) \end{aligned} \quad (2)$$

where i and j represent the micromagnetic unit cells, and p, q represent the Cartesian components of the thermal field. T_i and α_i denote temperature and the Gilbert damping at cell i , respectively, and a is the unit cell size. k_B is the Boltzmann constant. With the discrete time step Δt , the thermal/random field can be represented as

$$h_{\text{th},i,p} = \eta \sqrt{\frac{2\alpha k_B T}{\gamma \mu_0 M_s a^3 \Delta t}} \quad (3)$$

where η is a random number which satisfies the normal distribution with zero average.

TG ($\nabla_x T$) generates magnetization deviation at different positions from their equilibrium orientations, and thus small transverse components m_y and m_z are obtained. The transverse components vary with local temperature and fluctuate spatially and temporally, which leads to a magnonic spin current [41]. The DW interacts with this magnonic spin current. Using the spin continuity equation obtained from equation (1), the spin current density along the x -direction due to exchange interaction, discarding the term of spin current containing the damping coefficient because of negligibly small contribution, is found as below (for details refer to [appendix](#))

$$\mathbf{J}(x) = \frac{2\gamma A}{\mu_0 M_s} \mathbf{m} \times \frac{\partial \mathbf{m}}{\partial x} \quad (4)$$

$\mathbf{J}(x)$ can be computed numerically [33, 50] from numerically simulated data. For lower damping, the spin current contributions from damping and thermal field are relatively small. In addition, importantly, the spin-current contribution (from the damping term) should neutralize the spin-current contribution (from the thermal field term) for an average over a longer time according to the fluctuation-dissipation theorem [46]. So, the net contribution of the damping term and the thermal field term is negligibly small.

To find the DW velocity, v_{nsc} from the net spin current density, the x -component of equation (A4) is integrated over a space which encloses the DW at the center,

$$v_{\text{nsc}} = \frac{1}{2} \int_{-L_x/2}^{L_x/2} \frac{\partial m_x}{\partial t} dx \quad (5)$$

$$= -\frac{1}{2} (J_{x;\text{left}} - J_{x;\text{right}}) \quad (6)$$

where the fluctuations in the domains are assumed to be small. $J_{x;\text{left}}, J_{x;\text{right}}$ represent the x -components of the spin current on the left- and right-sides of the DW. The equation (6) clearly reveals that the DW will move opposite to the spin current direction.

3. Numerical results

We first investigate the DW dynamics in the nanowire of length $L_x = 2048 \text{ nm}$ under TG, $\nabla_x T$. Purposely, 15 random trajectories of DW propagation are simulated for each $\nabla_x T$ while

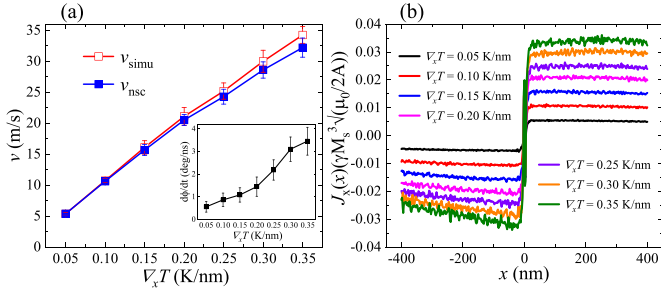


Figure 2. The model parameters are $M_s = 8 \times 10^5 \text{ A m}^{-1}$, $A = 13 \times 10^{-12} \text{ J m}^{-1}$, $\alpha = 0.002$ and $K_x = 500 \text{ J m}^{-3}$. With the configuration $L_x = 2048 \text{ nm}$, $L_y = L_z = 4 \text{ nm}$ (a) DW velocity v_{simu} obtained from simulations (red line) and v_{nsc} computed from the net spin current (blue line) as a function of $\nabla_x T$. Inset: TG dependence of DW rotational velocity (black line). (b) The spatial dependence of spin current densities $J_x(x)$ for various $\nabla_x T$. $x = 0$ is chosen as the DW center.

other parameters are kept fixed. Then we take the statistical ensemble average to obtain the time-dependent average DW position, and hence DW velocity v_{simu} and rotational velocity ($d\phi/dt$, where ϕ is tilted angle of DW-plane) are estimated. It is observed that the DW moves toward the hotter region accompanying DW-plane rotation around the easy x -axis. The DW-plane of head-to-head DW (tail-to-tail DW) rotates counter-clock (clock) wise around the x -axis during DW propagation. Figure 2(a) shows v_{simu} (red line) as a function $\nabla_x T$ while inset of figure 2(a) demonstrates $d\phi/dt$ (black line) with $\nabla_x T$. The DW speeds change with $\nabla_x T$ linearly. The Walker breakdown limit is absent as the uniaxial nanowire is studied here.

Later on, we calculate DW velocity v_{nsc} from the net spin current density $J_x(x)$, which comes from the TSWs only. Purposely, the $J_x(x)$ is calculated using the equation (4). Figure 2(b) shows the spatial distribution of $J_x(x)$ (ensemble averaged) with DW at the center $x = 0$ for different TGs. At the DW center, the sign of the spin current density $J_x(x)$ is suddenly changed, which indicates the evidence of angular-momentum transfer from the spin current to the DW. The spin current polarization alters its sign since the magnetizations of the two domains are separated by the DW in the opposite directions. In order to calculate the DW speed v_{nsc} from spin current $J_x(x)$ (using equation (6)), we take the averages of $J_x(x)$ over $x \in [-2\Delta, -\Delta]$ and $x \in [\Delta, 2\Delta]$ while Δ is referred to the DW width which is 60 nm in this study.

The v_{nsc} (blue line) as a function of TG is presented in figure 2(a). It is mentioned that v_{nsc} almost coincides with the simulated velocity v_{simu} (open squares) estimated directly from the DW propagation with time along x -direction. However, there is a small discrepancy at a higher TG, which is attributed to the contribution from stochastic fields and the dipolar field. The above findings are similar and agree with the microscopic theory (magnonic STT) [32, 33, 36, 41, 42].

Then, we investigate, for fixed $\nabla_x T$, $L_x = 1024 \text{ nm}$, the DW dynamics as a function of damping coefficient α (ranging from

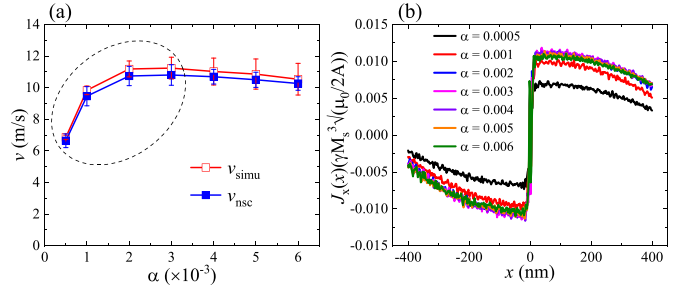


Figure 3. (a) DW velocity v_{simu} computed from simulations (red line) and v_{nsc} computed from the net spin current (blue line) as a function of α . (b) The spatial dependence of spin current densities $J_x(x)$ for varied α . $x = 0$ is chosen as the DW center. The model parameters in (a) and (b) are, $L_x = 1024 \text{ nm}$, $L_y = L_z = 4 \text{ nm}$, $\nabla_x T = 0.2 \text{ K nm}^{-1}$ and $K_x = 500 \text{ J m}^{-3}$.

0.0005 to 0.006). The obtained results of DW speed v_{simu} (red line) for different α are shown in figure 3(a). It is interestingly observed that the v_{simu} is smaller for lower damping ($\alpha \sim 0.0005$) and v_{simu} increases and becomes maximal for a certain α , referred to as critical damping α_c (indicated by the dotted circle in figure 3(a)) and then decreases monotonically with α . Usually, for the range 0.002 to 0.006, the decreasing trend of v_{simu} with α is desired since α compels the spin current polarization to align with the local spin, which reduces the magnon propagation length and hence the amount of spin angular momentum deposited on a DW is decreased with α . However, this study focuses on why v_{simu} is smaller for lower ($\alpha \sim 0.0005$) and v_{simu} increases and becomes maximal for a certain α , although the magnon propagation length is larger for lower α . To explain this observation, we recall the basic physics of generating SSWs in the nanowire with fixed boundaries. With the lower damping ($\alpha \sim 0.0005$), some modes of spin waves (whose propagation length is larger than the distance between two boundaries) can reflect from the boundary and superpose with the incoming spin waves and thus, the SSWs are formed together with the TSWs. It is well known that the SSW does not carry any net energy/momentum to DW, whereas TSW does. Consequently, with lower α , the amount of spin angular momentum deposited on a DW is reduced, and thus v_{simu} becomes smaller. Then if α gradually increases, the propagation length of spin waves reduces, and hence the SSW modes are converted to the TSW modes, i.e. the number of TSW modes which increases the DW speed. Therefore, for a certain α_c the SSW modes are fully converted to the TSW modes, and hence the DW speeds become maximum. Then for a further increment of α , the propagation length of the TSW decreases, and thus DW speed decreases with α monotonically because of the reduction of magnonic STT to the DW.

Furthermore, from the figure 3(a), it is noted that, for $\alpha < \alpha_c$, the slope (the rate of change of the DW velocity with damping) is larger than the slope for $\alpha > \alpha_c$. This observation indicates that the DW velocity reduction caused by the SSW is more significant than the spin current attenuation by damping.

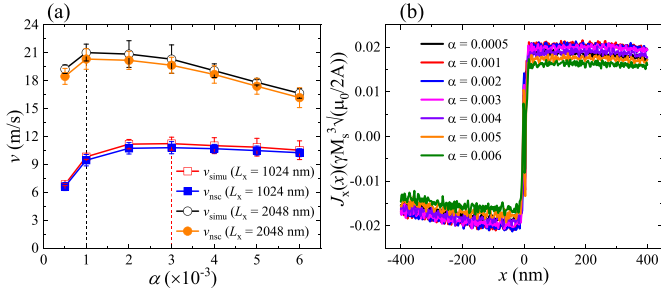


Figure 4. (a) Comparison of the damping-dependent DW velocity between $L_x = 1024$ nm (red line) and $L_x = 2048$ nm (black line). DW velocity v_{simu} (red/black lines) computed from micromagnetic simulations and v_{nsc} (orange/blue line) computed from the net spin current. (b) The spatial dependence of spin current densities $J_x(x)$ for varied α for $L_x = 2048$ nm. $x = 0$ is chosen as the DW center. The model parameters in (a) and (b) are, $L_x = 1024$ or 2048 nm, $L_y = L_z = 4$ nm, $\nabla_x T = 0.2$ K nm $^{-1}$ and $K_x = 500$ J m $^{-3}$.

To justify the above explanation numerically, it is required to separate the contribution of TSW modes from SSW modes. However, the expression of spin current density $J_x(x)$, refers to (4), which comes from the TSWs contribution. We can calculate the average $J_x(x)$ from simulated data, and hence DW velocity v_{nsc} can be calculated using the equation (6). So, we estimated the average spin current density $J_x(x)$, along x -direction (as described previously) for different α . The spatial distribution of $J_x(x)$ for different α are shown in figure 3(b). It is mentioned that the $J_x(x)$ is smaller for lower damping, and its value increases till a certain value and then decreases with α which was expected according to the above explanation. And thus, we find the DW speeds (blue line) v_{nsc} for different α , which are shown in figure 3(a). The DW speed v_{nsc} agrees well with the v_{simu} except small discrepancy that we have explained previously.

In order to give justification in terms of nanowire length by keeping the same $\nabla_x T = 0.2$ K nm $^{-1}$, i.e. by keeping the same propagation length of spin waves/magnons, we choose the longer length of the nanowire, since with the increase the distance between boundaries of the two ends, the generating of SSW modes would be reduced, and contrarily the TSW would be increased. Thus, the DW speed should be increased. Purposely, with the same $\nabla_x T = 0.2$ K nm $^{-1}$ and other parameters, we investigate DW dynamics in the nanowire of length, $L_x = 2048$ nm as a function of α (~ 0.001 to 0.006). In the figure 4(a), the black line (for $L_x = 2048$ nm) and the red line (for $L_x = 1024$ nm) show the comparison of DW speed as a function of α .

It is noted that DW speed is significantly larger for the length $L_x = 2048$ nm compared to the $L_x = 1024$ nm. Noticeably, for $L_x = 2048$ nm, DW speed increases till $\alpha = 0.001$ (maximal v_{simu} indicated by black dotted line), and then shows the usual decreasing trend with α . However, for $L_x = 1024$ nm, DW speed increases till $\alpha = 0.003$ (indicated by the red dotted line) and then decreases with α monotonically. That is, the critical point (at which v_{simu} is maximal) shifts to lower α , which is consistent with the explanation. These observations can be explained as, for fixed α , the number of SSWs is smaller

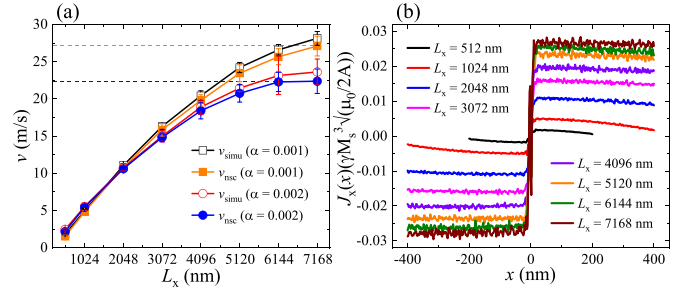


Figure 5. (a) Comparison of the length-dependent DW velocity between $\alpha = 0.001$ (black line) and $\alpha = 0.002$ (red line). DW velocity v_{simu} computed from micromagnetic simulations (black/red circles) and v_{nsc} computed from the net spin current (orange/blue circles). (b) The spatial dependence of spin current densities $J_x(x)$ for varied L_x for $\alpha = 0.001$. $x = 0$ is chosen as the DW center. The model parameters in (a) and (b) are, $L_y = L_z = 4$ nm, $\alpha = 0.001$ or 0.002 , $\nabla_x T = 0.1$ K nm $^{-1}$ and $K_x = 500$ J m $^{-3}$.

for longer $L_x = 2048$ nm and vice versa. This is why, with a small increment of α (e.g. 0.001) for $L_x = 2048$, the SSWs are eliminated, and DW speed becomes maximum, and then DW speed started to decrease with α as the usual trend. For $L_x = 2048$, we also estimated the $J_x(x)$ for different α , and the spatial distributions for different α are shown in figure 4(b). We find the DW speeds v_{nsc} (orange/blue line) for different α , which are shown in figure 4(a). The v_{nsc} (orange/blue line) agrees well with the v_{simu} (black/red line).

Previously, we found that v_{simu} increases with L_x . Therefore, it is expected that v_{simu} should be maximal for a certain length which is referred to as L_{xc} and larger than L_{xc} , the v_{simu} would be constant. We study the DW dynamics in the nanowire of $L_x = 512, 1024, 2048, 3072, 4096, 5120, 6144, 7168$ nm under $\nabla_x T = 0.1$ K nm $^{-1}$ for two different α . The obtained v_{simu} (black line for $\alpha = 0.001$ and red line for $\alpha = 0.002$) as a function of L_x are demonstrated in figure 5(a). In both cases, it is observed that v_{simu} increases gradually till a certain L_x and then becomes saturated to maximal speed (indicated by the horizontal dotted lines), which is expected. Since the number of SSWs gradually decreases, and the number of TSWs increases with L_x , DW speed increases. For each L_x , we also estimated the $J_x(x)$ for different L_x and the spatial distributions for different L_x are shown in figure 5(b). We find $J_x(x)$ increases with L_x , and thus the v_{nsc} (orange line for $\alpha = 0.001$ and blue line for $\alpha = 0.002$) increases with L_x which are shown in figure 5(a). The v_{nsc} agrees well with the v_{simu} as expected.

Lastly, we would like to see whether uniaxial anisotropy K_x affects the excited SSW modes. Purposely, we study, for fixed $\nabla_x T$, $L_x = 2048$ nm, the DW dynamics as a function of α for two different uniaxial anisotropy K_x i.e. 10^4 and 10^5 J m $^{-3}$. The obtained v_{simu} as a function of α are presented by red (for $K_x = 10^4$ J m $^{-3}$) and black (for $K_x = 10^5$ J m $^{-3}$) lines in the figure 6. In both cases, v_{simu} is maximal for $\alpha = 0.001$, i.e. damping dependence of v_{simu} for two different K_x shows similar trend. We can say uniaxial anisotropy K_x does not affect the formation/elimination of SSW modes which is expected as K_x is not related to the magnon

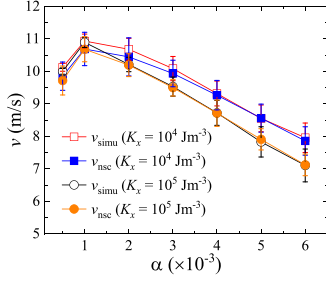


Figure 6. Damping dependence of DW speeds v_{simu} for $K_x = 10^4 \text{ J m}^{-3}$ (red line) and $K_x = 10^5 \text{ J m}^{-3}$ (black line). DW velocity v_{simu} computed from micromagnetic simulations (red/black line) and v_{nsc} computed from the net spin current (blue/orange line). The model parameters are, $L_x = 2048 \text{ nm}$, $L_y = L_z = 4 \text{ nm}$, and $\nabla_x T = 0.1 \text{ K nm}^{-1}$.

propagation length. However, for the damping range (0.001–0.006), v_{simu} are smaller for $K_x = 10^5 \text{ J m}^{-3}$ than that for $K_x = 10^4 \text{ J m}^{-3}$. This is because the larger K_x increases the energy gap, referring to the relation $\omega_{\mathbf{k}} = \frac{2\gamma}{\mu_0 M_s} (Ak^2 + K_x)$, where, k is the wavenumber. Thus, the number of magnons decreases since exciting magnons is harder. So, the spin current density decreases with the increase of K_x . To justify it, we estimated the v_{nsc} for different K_x (calculated from net spin current density) with varies damping and presented by blue (for $K_x = 10^4 \text{ J m}^{-3}$) and orange (for $K_x = 10^5 \text{ J m}^{-3}$) lines in the figure 6. The v_{spin} and v_{nsc} show good agreement.

4. Discussions and conclusions

Here we investigate the DW dynamics in uniaxial nanowires under TG. We found that the DW propagates toward the hotter region of the nanowire with accompanying DW-plane rotation around the easy axis. The DW (linear and rotational) speeds increase with TG linearly. These observations are similar to the studies [32, 33, 42], and the reason is attributed to the mechanism of the magnonic STT to the DW. Interestingly, we observed that the DW speed increases with α (for the range of $\alpha \sim 0.0005$ to 0.001) to a maximal value and then decrease, monotonically with α . Usually, the DW speed should decrease with α since the spin-wave/magnon propagation length is inversely proportional to α .

However, for a lower α , DW speed is smaller. This is because, with lower α , more SSW modes are formed (from the superposition of spin waves and their reflection at the boundary) rather than TSWs. The SSW does not carry any spin angular momentum/magnonic STT to the DW, while the TSW does. With the increment of α (from 0.0005 to 0.001), DW speed shows an increasing trend. This is because the magnon propagation length decreases with α , and thus α hinders the generation the SSWs, and, contrarily, the number of TSWs increases, which leads the increment of DW speed. We also observed that DW speed v_{simu} increases with L_x and becomes saturated to maximal (indicated by horizontal dotted lines) for a certain L_x . The reason is that the distance between two ends increases with L_x , which reduces the formation of the SSWs; contrarily, the number of TSWs increases and thus DW speed

increases. Similar findings are expected for the biaxial (rectangular cross-section) nanowire. Therefore, the above findings of DW dynamics in nanowires under TG may be useful for the fundamental understanding and to optimize the damping coefficient and nanowire length for applications in spintronics devices.

Data availability statement

All data that support the findings of this study are included within the article (and any supplementary files).

Acknowledgment

M T Islam acknowledges the National Key R&D Program of China (Grant No. 2022YFB4400200), Khulna University Research Cell (Grant No. KU/RC-04/2000-158), Khulna, Bangladesh, the Ministry of Education (BANBEIS, Grant No. SD2019972), Bangladesh, the Key Research and Development Program of Shaanxi Province (Grant No. 2021GXLH-Z-065) and the National Key R&D Program of China (Grant No. 2021YFA1202200) and X R Wang acknowledges the support of Hong Kong RGC Grant (Nos. 16300522 and 16302321).

Appendix. Calculation of $J_x(x)$ and v_{nsc}

In this appendix, we show the derivation of the spin current density $J_x(x)$ and the DW velocity v_{nsc} from spin current density in equation (6). The LLG equation is given by,

$$\frac{\partial \mathbf{m}}{\partial t} = -\gamma \mathbf{m} \times \mathbf{h}_{\text{eff}} + \alpha \mathbf{m} \times \frac{\partial \mathbf{m}}{\partial t} \quad (\text{A1})$$

where,

$$\mathbf{h}_{\text{eff}} = \frac{2A}{\mu_0 M_s} \frac{\partial^2 \mathbf{m}}{\partial x^2} + \frac{2K_x}{\mu_0 M_s} m_x \hat{x}. \quad (\text{A2})$$

Substituting the expression of $\frac{\partial \mathbf{m}}{\partial t}$ in the second term of equation (A1), we get,

$$(1 + \alpha^2) \frac{\partial \mathbf{m}}{\partial t} = -\gamma \mathbf{m} \times \mathbf{h}_{\text{eff}} - \alpha \gamma (\mathbf{m} \times \mathbf{m} \times \mathbf{h}_{\text{eff}}). \quad (\text{A3})$$

Now, substituting the expression of \mathbf{h}_{eff} from equation (A2) in equation (A3), we get,

$$\begin{aligned} (1 + \alpha^2) \frac{\partial \mathbf{m}}{\partial t} &= -\gamma \mathbf{m} \times \left[\frac{2A}{\mu_0 M_s} \frac{\partial^2 \mathbf{m}}{\partial x^2} + \frac{2K_x}{\mu_0 M_s} m_x \hat{x} \right] \\ &\quad - \alpha \gamma \left(\mathbf{m} \times \mathbf{m} \times \left[\frac{2A}{\mu_0 M_s} \frac{\partial^2 \mathbf{m}}{\partial x^2} + \frac{2K_x}{\mu_0 M_s} m_x \hat{x} \right] \right) \\ &= -\frac{2\gamma A}{\mu_0 M_s} \left(\mathbf{m} \times \frac{\partial^2 \mathbf{m}}{\partial x^2} \right) - \frac{2\gamma K_x}{\mu_0 M_s} m_x (\mathbf{m} \times \hat{x}) \\ &\quad - \frac{2\alpha \gamma A}{\mu_0 M_s} \left(\mathbf{m} \times \mathbf{m} \times \frac{\partial^2 \mathbf{m}}{\partial x^2} \right) - \frac{2\alpha \gamma K_x}{\mu_0 M_s} m_x (\mathbf{m} \times \mathbf{m} \times \hat{x}) \end{aligned}$$

$$\begin{aligned}
&= -\frac{2\gamma A}{\mu_0 M_s} \frac{\partial}{\partial x} \left(\mathbf{m} \times \frac{\partial \mathbf{m}}{\partial x} \right) - \frac{2\gamma K_x}{\mu_0 M_s} m_x (\mathbf{m} \times \hat{x}) \\
&\quad - \frac{2\alpha\gamma A}{\mu_0 M_s} \left[\mathbf{m} \times \frac{\partial}{\partial x} \left(\mathbf{m} \times \frac{\partial \mathbf{m}}{\partial x} \right) \right] \\
&\quad - \frac{2\alpha\gamma K_x}{\mu_0 M_s} m_x [\mathbf{m}(\mathbf{m} \cdot \hat{x}) - \hat{x}(\mathbf{m} \cdot \mathbf{m})] \\
&= -\frac{\partial \mathbf{J}}{\partial x} - \frac{2\gamma K_x}{\mu_0 M_s} m_x (\mathbf{m} \times \hat{x}) - \alpha \left(\mathbf{m} \times \frac{\partial \mathbf{J}}{\partial x} \right) \\
&\quad - \frac{2\alpha\gamma K_x}{\mu_0 M_s} (m_x^2 - 1) m_x \hat{x} - \frac{2\alpha\gamma K_x}{\mu_0 M_s} m_x m_x^2 m_y \hat{y} + \frac{2\alpha\gamma K_x}{\mu_0 M_s} m_x^2 m_z \hat{z}
\end{aligned}$$

where, $\mathbf{J}(x) = \frac{2\gamma A}{\mu_0 M_s} \mathbf{m} \times \frac{\partial \mathbf{m}}{\partial x}$ is magnetization current due to exchange interaction, also referred as the spin-wave spin current [33] which can be calculated from the simulated data. For lower damping, i.e. $\alpha \sim 0.0005-0.006$, the terms multiplied with damping coefficient are neglected and $(1 + \alpha^2) = 1$.

By taking the x -components of the above equation, we obtain,

$$\frac{\partial m_x}{\partial t} = -\frac{\partial J_x}{\partial x}. \quad (\text{A4})$$

The DW position is defined as,

$$\begin{aligned}
x(t) &= \frac{L_x}{2} (\langle m_x \rangle + 1) \\
\Rightarrow \frac{\partial x(t)}{\partial t} &= v_{\text{simu}} = \frac{L_x}{2} \frac{\partial \langle m_x \rangle}{\partial t}
\end{aligned}$$

where, v_{simu} is the DW velocity calculated from the change of DW position.

The average value of m_x is,

$$\langle m_x \rangle = \int_{-L_x/2}^{L_x/2} \frac{1}{L_x} m_x dx.$$

Now,

$$\begin{aligned}
v_{\text{simu}} &= \frac{L_x}{2} \frac{\partial}{\partial t} \int_{-L_x/2}^{L_x/2} \frac{1}{L_x} m_x dx \\
\Rightarrow v_{\text{nsc}} &= \frac{1}{2} \int_{-L_x/2}^{L_x/2} \frac{\partial m_x}{\partial t} dx \\
\Rightarrow v_{\text{nsc}} &= -\frac{1}{2} \int_{-L_x/2}^{L_x/2} \frac{\partial J_x}{\partial x} dx \\
\Rightarrow v_{\text{nsc}} &= -\frac{1}{2} (J_{x:\text{left}} - J_{x:\text{right}})
\end{aligned}$$

where, v_{nsc} is the DW velocity calculated from the net spin current density.

ORCID iDs

M A S Akanda  <https://orcid.org/0000-0002-6742-2158>

M T Islam  <https://orcid.org/0000-0002-3846-4009>

References

- [1] Parkin S S, Hayashi M and Thomas L 2008 Magnetic domain-wall racetrack memory *Science* **320** 190
- [2] Tsoi M, Fontana R and Parkin S 2003 Magnetic domain wall motion triggered by an electric current *Appl. Phys. Lett.* **83** 2617
- [3] Grollier J, Boulenc P, Cros V, Hamzić A, Vaures A, Fert A and Faini G 2003 Switching a spin valve back and forth by current-induced domain wall motion *Appl. Phys. Lett.* **83** 509
- [4] Allwood D, Xiong G, Cooke M, Faulkner C, Atkinson D, Vernier N and Cowburn R 2002 Submicrometer ferromagnetic not gate and shift register *Science* **296** 2003
- [5] Allwood D A, Xiong G, Faulkner C, Atkinson D, Petit D and Cowburn R 2005 Magnetic domain-wall logic *Science* **309** 1688
- [6] Schryer N L and Walker L R 1974 The motion of 180 domain walls in uniform dc magnetic fields *J. Appl. Phys.* **45** 5406
- [7] Wang X R, Yan P, Lu J and He C 2009 Magnetic field driven domain-wall propagation in magnetic nanowires *Ann. Phys., NY* **324** 1815
- [8] Wang X R, Yan P and Lu J 2009 High-field domain wall propagation velocity in magnetic nanowires *Europhys. Lett.* **86** 67001
- [9] Atkinson D, Allwood D A, Xiong G, Cooke M D, Faulkner C C and Cowburn R P 2003 Magnetic domain-wall dynamics in a submicrometre ferromagnetic structure *Nat. Mater.* **2** 85
- [10] Beach G S, Nistor C, Knutson C, Tsoi M and Erskine J L 2005 Dynamics of field-driven domain-wall propagation in ferromagnetic nanowires *Nat. Mater.* **4** 741
- [11] Jing K, Gong X and Wang X 2022 Field-driven domain wall motion in ferrimagnetic nanowires *Phys. Rev. B* **106** 174429
- [12] Sun Z and Wang X R 2006 Magnetization reversal through synchronization with a microwave *Phys. Rev. B* **74** 132401
- [13] Moriyama T, Cao R, Xiao J Q, Lu J, Wang X R, Wen Q and Zhang H 2007 Microwave-assisted magnetization switching of Ni₈₀Fe₂₀ in magnetic tunnel junctions *Appl. Phys. Lett.* **90** 152503
- [14] Yan P and Wang X R 2009 Domain wall propagation due to the synchronization with circularly polarized microwaves *Phys. Rev. B* **80** 214426
- [15] Han D-S, Kim S-K, Lee J-Y, Hermsdoerfer S J, Schultheiss H, Leven B and Hillebrands B 2009 Magnetic domain-wall motion by propagating spin waves *Appl. Phys. Lett.* **94** 112502
- [16] Yamaguchi A, Ono T, Nasu S, Miyake K, Mibu K and Shinjo T 2004 Real-space observation of current-driven domain wall motion in submicron magnetic wires *Phys. Rev. Lett.* **92** 077205
- [17] Yamaguchi A, Hirohata A, Ono T and Miyajima H 2011 Temperature estimation in a ferromagnetic Fe-Ni nanowire involving a current-driven domain wall motion *J. Phys.: Condens. Matter* **24** 024201
- [18] Kim S K, Beach G S, Lee K-J, Ono T, Rasing T and Yang H 2022 Ferrimagnetic spintronics *Nat. Mater.* **21** 24
- [19] Xing X and Zhou Y 2022 Skyrmion motion and partitioning of domain wall velocity driven by repulsive interactions *Commun. Phys.* **5** 241
- [20] Hayashi M, Thomas L, Bazaliy Y B, Rettner C, Moriya R, Jiang X and Parkin S 2006 Influence of current on field-driven domain wall motion in permalloy nanowires from time resolved measurements of anisotropic magnetoresistance *Phys. Rev. Lett.* **96** 197207
- [21] Berger L 1996 Emission of spin waves by a magnetic multilayer traversed by a current *Phys. Rev. B* **54** 9353
- [22] Slonczewski J C 1996 Current-driven excitation of magnetic multilayers *J. Magn. Magn. Mater.* **159** L1

- [23] Zhang S and Li Z 2004 Roles of nonequilibrium conduction electrons on the magnetization dynamics of ferromagnets *Phys. Rev. Lett.* **93** 127204
- [24] Tataru G and Kohno H 2004 Theory of current-driven domain wall motion: spin transfer versus momentum transfer *Phys. Rev. Lett.* **92** 086601
- [25] Jung S-W, Kim W, Lee T-D, Lee K-J and Lee H-W 2008 Current-induced domain wall motion in a nanowire with perpendicular magnetic anisotropy *Appl. Phys. Lett.* **92** 202508
- [26] Bauer G E, Saitoh E and Van Wees B J 2012 Spin caloritronics *Nat. Mater.* **11** 391
- [27] Jiang W et al 2013 Direct imaging of thermally driven domain wall motion in magnetic insulators *Phys. Rev. Lett.* **110** 177202
- [28] Le Breton J-C, Sharma S, Saito H, Yuasa S and Jansen R 2011 Thermal spin current from a ferromagnet to silicon by seebeck spin tunnelling *Nature* **475** 82
- [29] Uchida K, Takahashi S, Harii K, Ieda J, Koshibae W, Ando K, Maekawa S and Saitoh E 2008 Observation of the spin seebeck effect *Nature* **455** 778
- [30] Wang X R, Yan P and Wang X S 2012 Magnonic spin-transfer torque and domain wall propagation *IEEE Trans. Magn.* **48** 4074
- [31] Safranski C et al 2017 Spin caloritronic nano-oscillator *Nat. Commun.* **8** 1
- [32] Wang X G, Guo G H, Nie Y Z, Zhang G F and Li Z X 2012 Domain wall motion induced by the magnonic spin current *Phys. Rev. B* **86** 054445
- [33] Yan P, Wang X S and Wang X R 2011 All-magnonic spin-transfer torque and domain wall propagation *Phys. Rev. Lett.* **107** 177207
- [34] Kovalev A A and Tserkovnyak Y 2012 Thermomagnonic spin transfer and peltier effects in insulating magnets *Europhys. Lett.* **97** 67002
- [35] Kim S K and Tserkovnyak Y 2015 Landau-Lifshitz theory of thermomagnonic torque *Phys. Rev. B* **92** 020410
- [36] Yan P, Cao Y and Sinova J 2015 Thermodynamic magnon recoil for domain wall motion *Phys. Rev. B* **92** 100408
- [37] Schlickeiser F, Ritzmann U, Hinzke D and Nowak U 2014 Role of entropy in domain wall motion in thermal gradients *Phys. Rev. Lett.* **113** 097201
- [38] Etesami S, Chotorlishvili L, Sukhov A and Berakdar J 2014 Longitudinal spin current induced by a temperature gradient in a ferromagnetic insulator *Phys. Rev. B* **90** 014410
- [39] Wang X S and Wang X R 2014 Thermodynamic theory for thermal-gradient-driven domain-wall motion *Phys. Rev. B* **90** 014414
- [40] Raimondo E, Saugar E, Barker J, Rodrigues D, Giordano A, Carpentieri M, Jiang W, Chubykalo-Fesenko O, Tomasello R and Finocchio G 2022 Temperature-gradient-driven magnetic skyrmion motion *Phys. Rev. Appl.* **18** 024062
- [41] Hinzke D and Nowak U 2011 Domain wall motion by the magnonic spin seebeck effect *Phys. Rev. Lett.* **107** 027205
- [42] Islam M T, Wang X S and Wang X R 2019 Thermal gradient driven domain wall dynamics *J. Phys.: Condens. Matter* **31** 455701
- [43] Moretti S, Raposo V, Martinez E and Lopez-Diaz L 2017 Domain wall motion by localized temperature gradients *Phys. Rev. B* **95** 064419
- [44] Wang W, Albert M, Beg M, Bisotti M-A, Chernyshenko D, Cortés-Ortuño D, Hawke I and Fangohr H 2015 Magnon-driven domain-wall motion with the Dzyaloshinskii-Moriya interaction *Phys. Rev. Lett.* **114** 087203
- [45] Chico J, Etz C, Bergqvist L, Eriksson O, Fransson J, Delin A and Bergman A 2014 Thermally driven domain-wall motion in Fe on W(110) *Phys. Rev. B* **90** 014434
- [46] Brown Jr W F 1963 Thermal fluctuations of a single-domain particle *Phys. Rev.* **130** 1677
- [47] Gilbert T L 2004 A phenomenological theory of damping in ferromagnetic materials *IEEE Trans. Magn.* **40** 3443
- [48] Vansteenkiste A, Leliaert J, Dvornik M, Helsen M, García-Sánchez F and Van Waeyenbergh B 2014 The design and verification of MuMax3 *AIP Adv.* **4** 107133
- [49] Hinzke D, Kazantseva N, Nowak U, Mryasov O N, Asselin P and Chantrell R W 2008 Domain wall properties of FePt: from Bloch to linear walls *Phys. Rev. B* **77** 094407
- [50] Wang X-G, Chotorlishvili L, Guo G-H, Sukhov A, Dugaev V, Barnaś J and Berakdar J 2016 Thermally induced magnonic spin current, thermomagnonic torques and domain-wall dynamics in the presence of Dzyaloshinskii-Moriya interaction *Phys. Rev. B* **94** 104410